Lowland Technology International 2018; 19 (4): 229-236
International Association of Lowland Technology (IALT): ISSN 1344-9656
Special Issue on: Kumamoto Earthquake & Disaster

Research Paper

Evaluation of seismically induced slope displacement by energy approach and applicability to a Case Study related to the 2016 Kumamoto Earthquake

T. Ishizawa [1] and T. Kokusho [2]

ARTICLE INFORMATION

Article history:

Received: 06 March, 2017
Received in revised form: 17 January, 2018
Accepted: 19 January, 2018
Publish on: 09 March, 2018

Keywords:

Energy balance
Earthquake energy
Slope failure
Residual displacement
Friction coefficient

ABSTRACT

The energy approach for slope failure evaluation has been developed by examining the energy balance in the rigid block model, comparing it to innovative shake table tests of sand model slope. As a result, previous studies have shown evaluation method is proposed in which residual slope displacement can be given from the earthquake energy. Moreover, a framework of performance-based design for slopes during earthquakes has been proposed. However, this energy method needs to have more research to upgrade the energy method to a reliable design tool. Therefore, the energy-based method was applied to a case history during the 2016 Kumamoto earthquake. The input earthquake energy defined as a base layer of the slope was extrapolated from several strong motion records. This paper discusses applicability of the energy-based method to a case history, during the 2016 Kumamoto earthquake, of the sliding-mass was travelled gentle slope along the clear slip plane, as a simplified rigid block model.

1. Introduction

Earthquake-induced slope stability has been evaluated by force-equilibrium of soil mass, though this force approach can't evaluate failure deformation once large failure occurs. It is very important to evaluate how large the deformation will develop and how far the effect reaches down-slope. Therefore, this study aims the development of evaluation method for residual slope displacement during earthquake in terms of energy.

In this study, an energy approach is proposed to evaluate slope failures including flow failures from their initiation to termination. The basic idea, first proposed in Kokusho et al. (2003), is shown in **Fig. 1.** In case of earthquake-induced slope failures, four energies; earthquake energy contributing to slope failure E_{EQ}, gravitational potential energy change $-\delta E_P$, dissipated energy in soil due to the slope deformation E_{DP} and kinetic energy E_K in a sliding soil mass, can be correlated as **Fig. 1.**

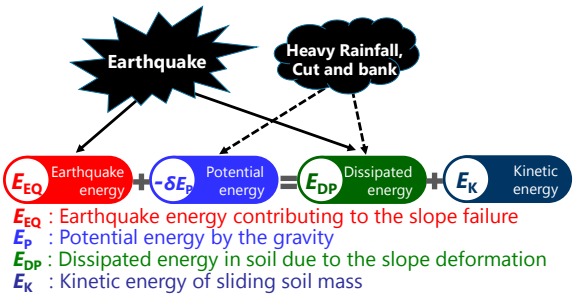

Fig. 1. Energy balance in flow failure of slopes (Kokusho et al., 2003).

[1] Chief Researcher, National Research Institute for Earth Science and Disaster Resilience, Ibaraki 305-0006, JAPAN, ishizawa@bosai.go.jp
[2] Professor Emeritus, Chuo University, Tokyo, JAPAN
Note: Discussion on this paper is open until September 2018.

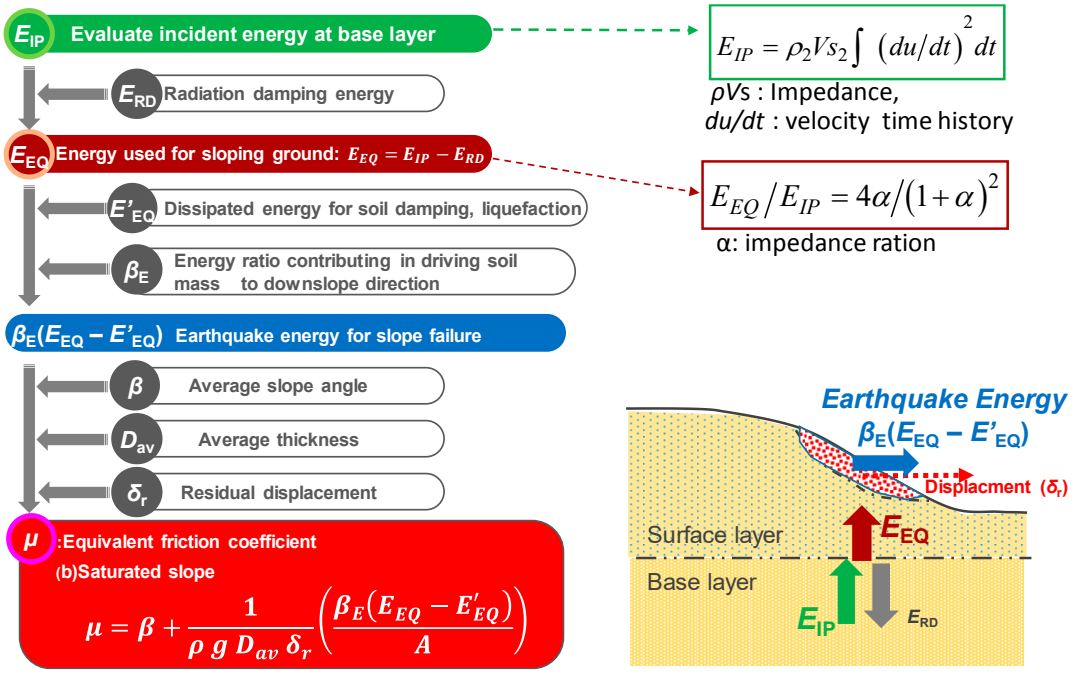

Fig. 2. Flow chart to back-calculate friction coefficient μ by energy approach.

The energy approach to slope failure evaluation has been developed by comparing the energy balance in a simplified rigid block model to results of shake table tests using the sand slope model. As a result, previous studies have shown that residual slope displacement δ_r can be given from the earthquake energy E_{EQ}, weight Mg, slope inclination β and friction coefficient μ by the following equation;

$$\delta_r = \frac{1+\mu\beta}{\mu-\beta} \cdot \frac{E_{EQ}}{Mg} \qquad [1a]$$

This equation is applicable to unsaturated slope where seismic inertia affects not only driving force but also shear resistance along the slip plane. If a slip plane is saturated, then the following equation should be used based on Eq. [1a].

$$\delta_r = \frac{1}{\mu-\beta} \cdot \frac{E_{EQ}}{Mg} \qquad [1b]$$

Furthermore, if an appropriate friction coefficient is chosen, **Eqs. [1a]** and **[1b]** by a simplified rigid block model can successfully simulate residual slope displacement δ_r.

In order to know how friction coefficient μ should be determined in actual design, friction coefficient μ in **Eq.(1b)** is back-calculated from a case history related to the 2016 Kumamoto earthquake in this study.

2. Back-calculate friction coefficient by energy approach

Figure 2 shows flow chart to back-calculate friction coefficient μ by energy approach.

First, the input earthquake energy E_{IP} defined at the base of slopes is designated site by site (Kokusho et al (2003)). The input energy E_{IP} can be evaluated as;

$$E_{IP} = \rho V_s \int (du/dt)^2 dt \qquad [2]$$

where du/dt is the particle velocity of the design motions in terms of time t and $\rho \cdot V_S$ is the impedance of the base layer. By assuming the energy radiating downward through the base, the earthquake energy E_{IP} can be obtained as;

$$E_{EQ}/E_{IP} = 4\alpha/(1+\alpha)^2 \qquad [3]$$

Thus, the energy ratio is controlled by the impedance ratio α between the sloping ground and a base layer (Kokusho et al. 2007). The energy E'_{EQ} is dissipated by residual slope deformation by internal soil damping in the sloping layer. The energy E'_{EQ} is seems small compared to E_{EQ}.

Next, by assuming the energy ratio β_E contributing to driving soil mass for downslope direction, the earthquake energy $\beta_E(E_{EQ} - E'_{EQ})$ to be used for the residual slope deformation can be differentiated (Kokusho et al. 2014).

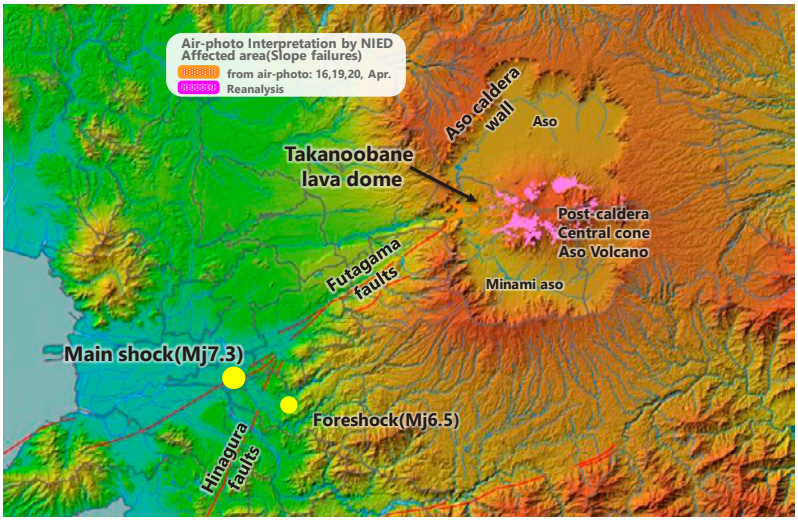

Fig. 3. Locations of slope failures and the epicenter of the 2016 Kumamoto earthquake (Based on Map by Geospatial Information Authority of Japan(GIA)).

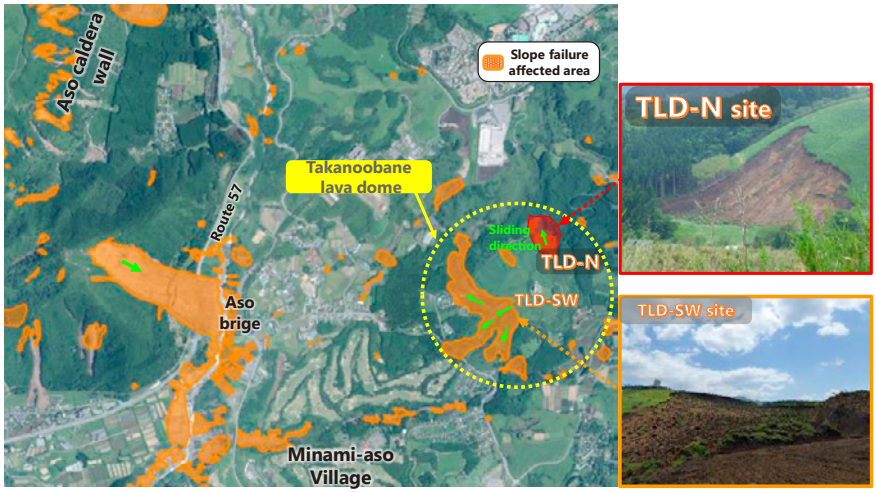

Fig. 4. Locations of slope failures around the Takanoobane lava dome of the 2016 Kumamoto earthquake (Based on photograph by Geospatial Information Authority of Japan(GIA)).

Based on the rigid-block simple model, Eq. [1b] is expressed here to back calculate equivalent friction coefficient μ $\left(\mu = \tan\phi_{eq}\right)$ as;

$$\mu = \beta + \frac{1}{\rho g D_{av} \delta_r}\left\{\frac{\beta_E\left(E_{EQ} - E'_{EQ}\right)}{A}\right\} \qquad [4]$$

where ϕ_{eq} is equivalent friction angle, A is horizontal area, D_{av} is thickness and ρg is unit weight of failed slope.

3. Case study related to the 2016 Kumamoto earthquake

3.1 2016 Kumamoto earthquake

The Kumamoto earthquake (M_J= 7.3, M_W= 7.0) in Japan occurred on April 16, 2016, which caused more than 700 slope failures. **Fig. 3.** shows the locations of slope failures and the epicenter of the 2016 Kumamoto earthquake.

In particular, the damaged area by numerous slope failures are located around Minami-aso Village at the Aso caldera western side. In those areas, the pumice, scoria, ash, igneous and volcanic-rock are distributed. The specificity of slope failures is categorized into three types in this earthquake.

- Type-A: Displaced soil mass travelled gentle slope along the clear slip plane (around central cones of Post-Aso volcano area).
- Type-B: Shallow landslides occurred at the steep slope (around caldera walls and central cones of Post-Aso volcano area).
- Type-C: Mudflow of displaced soil mass triggered earthquake ran down long distance (around central cones of Post-Aso volcano area).

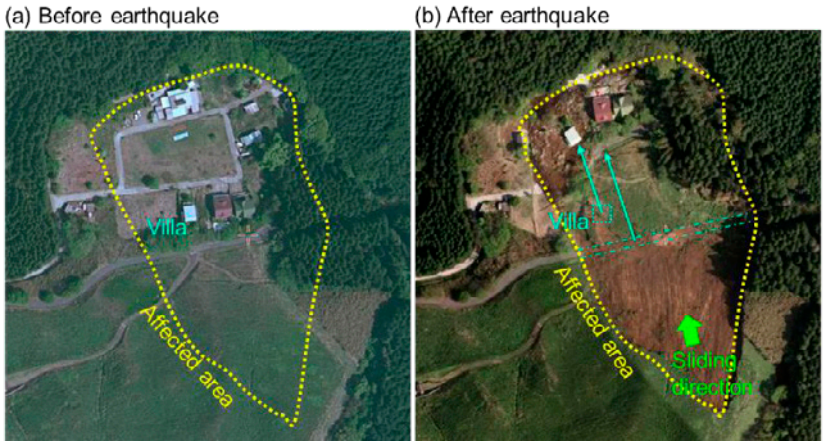

Fig. 5. Air-photograph of TLD-N slide before(a) and after(b) the earthquake (Based on photographs by Geospatial Information Authority of Japan(GIA)).

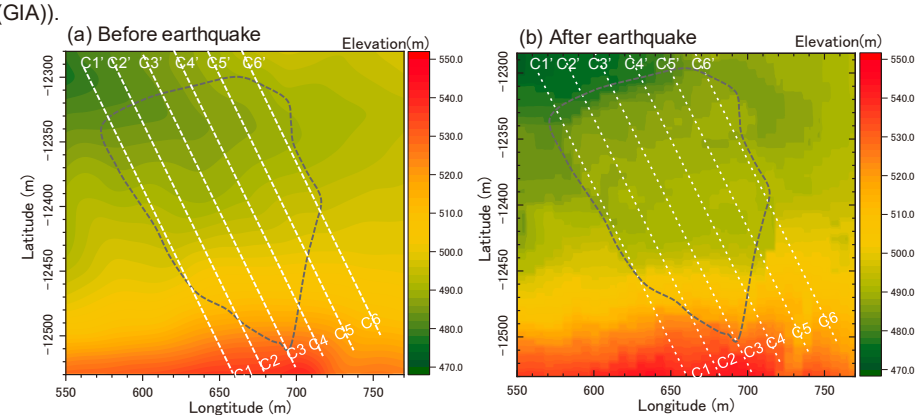

Fig. 6. Contour map of TLD-N slide before(a) and after(b) the earthquake.

3.2 Gentle slope failure at the Takanoobane lava dome

The most representative example of failure Type-A was occurred at the Takanoobane Volcano (lava dome). **Fig. 4** shows the locations of two slope failures (TLD-SW and TLD-N site in **Fig. 4**) at the Takanoobane lava dome. Two slope failures were occurred not only on steep slopes but also on gentle slopes. Sliding masses of largest slope failure, TLS-SW site: slope inclination about 10 degrees, travelled a long distance more than 500m, destroyed numerous houses and killed five people.

The northwest sliding slope failure, TLD-N site in **Fig. 4**, a failed soil mass slid down as a block along the clearly slip plane. This soil mass travelled more than 70m together with house in staying two residents related to the earthquake, and residents have no injury (in **Fig. 5**).

According to our field investigation after the earthquake, the slip surface of slope failures observed not volcanic rock (Takanoobane lava, Rhyolitic lava) but unconsolidated pyroclastic fall deposits shallower than volcanic rock layer. In this connection, it can be presumed that a slip plane contributing to driving soil mass is a pumice layer (Kpfa) at TLD-SW site, which a volcanic ash deeper than Kpfa layer at TDL-N site.

Figure 6 shows the contour map of TDL-N site slide (a) before and (b)after the earthquake. The ground surface elevations before the earthquake was obtained from Geospatial Information Authority of Japan. The post-earthquake elevation was obtained by DEM data based on 3D laser survey carried out on May 2016, about a month after the earthquake. Typical cross-sections along the 3 lines in **Figs. 6(a)** and **6(b)** are illustrated in **Fig. 7**.

The idealized block model is depicted in **Fig. 8**. The inclinations of the slope and slip plane were about 23.1 degrees. A soil block of 7.2 m in maximum depth and 75 m × 99 m in maximum horizontal dimensions slid along the sedimentation plane. The total volume of displaced soil calculated 3-dimensionally was 5.1×10^4 m^3 and 5.7×10^4 m^3 before and after the failure, respectively.

The simplification block model is slightly different from the real slip surface and the volume of slipped-mass. However, this paper focused on the movement of the center of gravity position. In order to reduce the position error of the center of gravity, the position of the center of gravity was calculated from the weighted mean of the soil mass. The failure was idealized here by simplifying the soil mass by a flat block of 7.5×10^3 m^2 (in horizontal area) by 7.2 m (in thickness) slipping down along the slip plane with the total

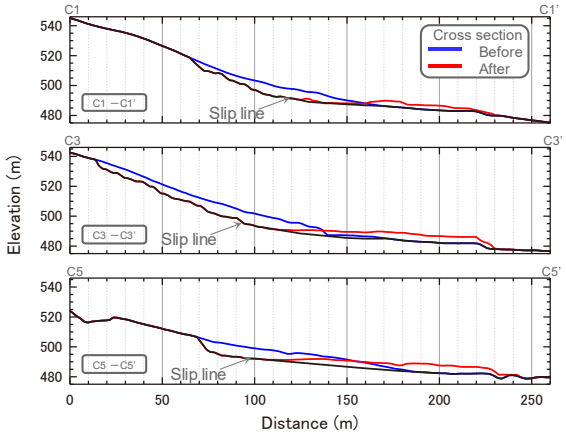

Fig. 7. Cross-sectional change of TLD-N slide before and after the earthquake.

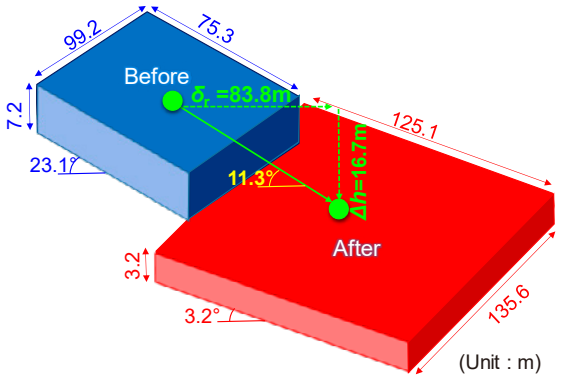

Fig. 8. Idealization of the TLD-N slide by rigid block model.

mass unchanged. The center of gravity moved by 83.8m laterally and 16.7m vertically. The equivalent slip inclination connecting the center of gravity before and after the failure is 11.3°, which is considerably lower than about 23.1°.

3.3 Estimate of earthquake energy for slope failure

Here, it was applied this energy evaluation method to the slope failure on northern side slope (TLD-N site) at the Takanoobane Volcano (lava dome) for an example.

First of all, the input earthquake energy E_{IP} defined at a base layer of the slope was extrapolated from several acceleration time histories. **Figure 9** shows the locations of strong motion stations (KiK-net) around slope failures together with the epicenter of the mainshock. The digitized acceleration time histories of the main shock recorded are available at NIED websites (http://www.kyoshin.bosai.go.jp/). It calculated the input energy E_{IP} with multiple vertical array records of the main shock, in Eq. [2].

For example, **Fig. 10(a)** shows the time-history of velocity record and input energies per unit area E_{IP}/A at the base layer of KMMH06 site (KiK-net: Hakusui). KMMH06 observation site is a nearest site to the TLD-N site. The time-history of the input energy per unit area E_{IP}/A at the

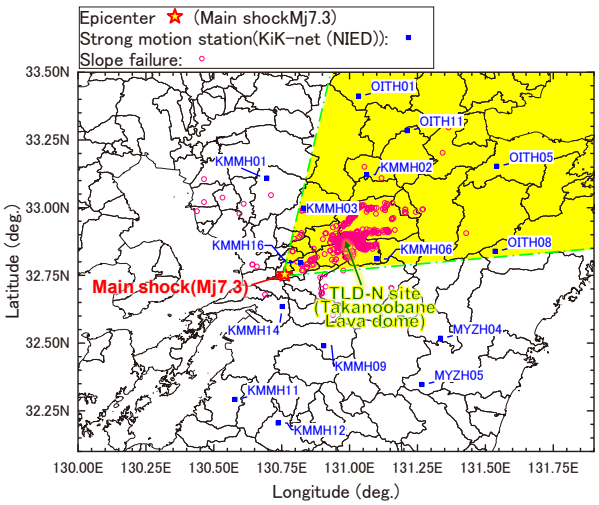

Fig. 9. Locations of strong motion stations, slope failures and the epicenter of the 2016 Kumamoto earthquake.

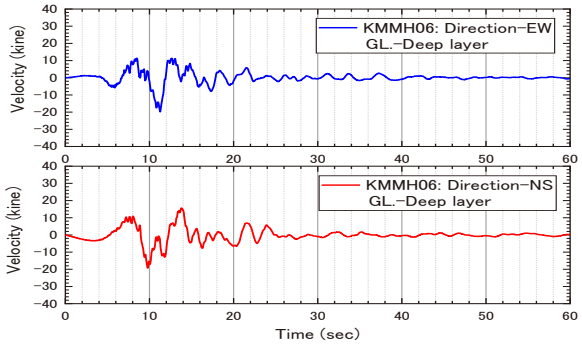

(a) Strong motion velocity record at base layer

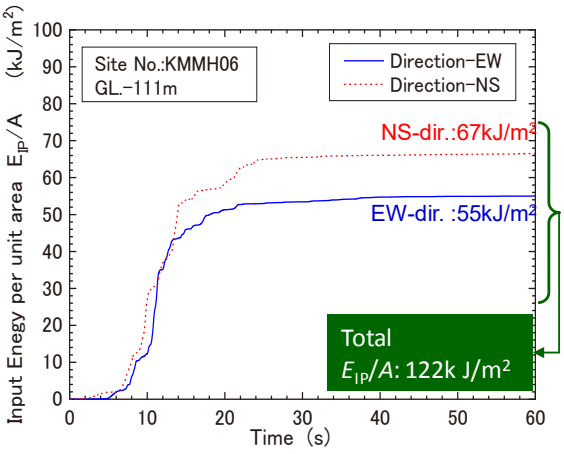

(b) Input energies per unit area E_{IP}/A at the base layer

Fig. 10. Time-history of velocity record and input energies per unit area E_{IP}/A at the base layer of KMMH06 site (KiK-net).

base layer of KMMH06 site calculated by Eq. [2] is shown in **Fig. 10(b)**. The total energy in the EW and NS directions is 122 kJ/m^2.

Figure 11 shows the calculated input energy per unit area E_{IP}/A at the base layers (about 100-250m deep) at the 15 sites, the values of E_{IP}/A are plotted versus hypocentral distance R (focal depth R_0 of the main shock: R_0 =

12 km). The dashed line in the chart indicates the wave energy per unit area theoretically calculated for M_J=7.3 from the spherical energy radiation of body waves,

$$E_{IP}/A = E/(4\pi R^2) \quad [5]$$

The total wave energy E released at a point source is evaluated by an empirical equation of Gutenberg and Richter (1956),

$$\log E = 1.5M + 11.8 \quad [6]$$

where M is the earthquake magnitude. Eqs.[5], [6] means the Input energy has affected by the hypocentral distance.

The input energy calculated from earthquake records tends to change the dashed line (M=7.3) in the chart because this simple formula disregards fault mechanism such as fault type, dimensions, directivity and asperity. However, when the calculated energy puts its focus on KiK-net sites of northeast direction from the epicenter, input energy E_{IP}/A can be approximated by the solid line for M=7.1.

Next, if the impedance ratio $\alpha = 0.3$ (Kokusho et al. 2011) and the energy ration contributing to downslope direction $\beta_E = 0.25$ (Kokusho et al. 2014) were assumed, then the earthquake energy for slope failure $\beta_E\left(E_{EQ} - E'_{EQ}\right)/A$ as previously mentioned from **Figure 2**.

$$\frac{\beta_E\left(E_{EQ}-E'_{EQ}\right)}{A} = \frac{\beta_E\left\{\left[4\alpha/(1+\alpha)^2\right]E_{IP}-E'_{EQ}\right\}}{A} \cong 0.18\left(E_{IP}/A\right) \quad [7]$$

In Eq.[7], internal dissipating energy E'_{EQ} by soil damping is assumed negligibly small compared to other energies.

The input energy at the base layer of TLD-N site(hypcentral distance: R = 28.1 km) which is assumed to have by the solid line in **Fig. 11** as E_{IP}/A = 284 kJ/m^2, hence, the maximum earthquake energy for the slope failure in TLD-N site was $\beta_E\left(E_{EQ} - E'_{EQ}\right)/A$ = 50 kJ/m^2.

3.4 Equivalent friction coefficients by back-calculated from slope failure

Estimating that the slip plane was saturated during earthquake and was a soil density ρ = 1.8 t/m^3 of failed soil mass, assuming that the major portion of the slid soil block was unsaturated except along the slip plane, Eq.[4] is expressed to back calculate equivalent friction coefficient μ or equivalent friction angle ϕ_{eq}. Then, the substituting equivalent friction coefficient μ (=tanϕ_{eq}=0.21) into Eq.[4], the equivalent friction angle ϕ_{eq} is 11.7°. This value corresponds to equivalent friction coefficient representing failure modes such as the rigid block slide along the smooth

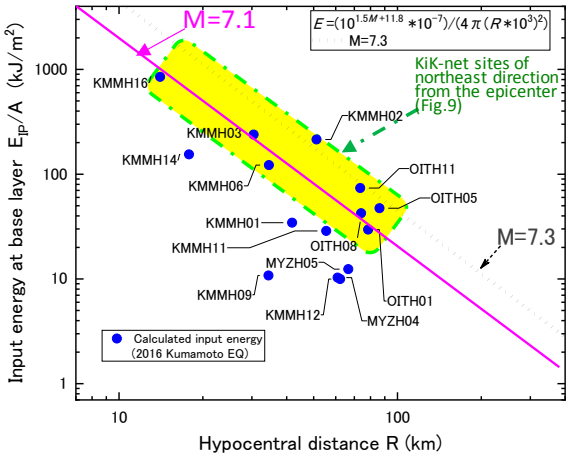

Fig. 11. Incident seismic wave energy versus hypocentral distance calculated from vertical array records, compared to a simple theory of spherical energy radiation.

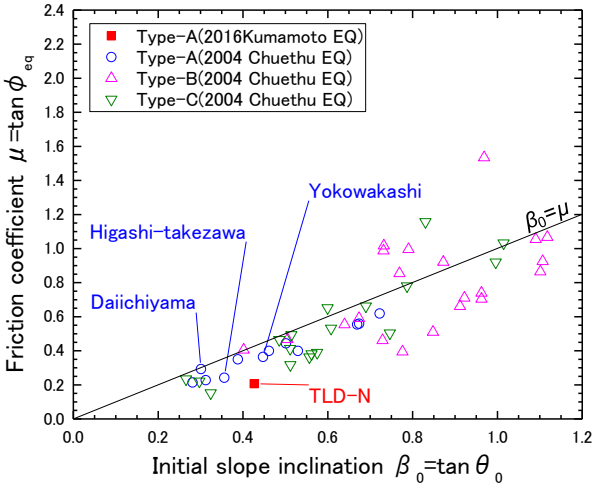

Fig. 12. Back-calculated friction coefficients versus initial slope inclinations.

slip plane, the crash and pile-up in the front, etc. This equivalent friction angle is much lower than the initial slope inclination $\beta_0 = \tan(\theta_0) = 0.43, \theta_0 = 23.1°$), indicating that the failed soil mass first accelerated and then decelerated due to gentler in down-slope sections.

Figure 12 illustrates the initial slope inclination β is plotted versus the friction coefficients back-calculated from the case histories. In this chart, it is shown the equivalent friction coefficients by back-calculated from slope failures during 2004 Niigata-ken Chuetu earthquake (M_J = 6.8). It is noted that those equivalent friction coefficients of Type-A (including TLR-N site) are much lower than initial slope inclinations.

In **Fig. 13**, the energy ratio, the potential energy $-\delta E_P/A$ divided by earthquake energy for slope failure $\beta_E\left(E_{EQ} - E'_{EQ}\right)/A$, are plotted the travel distance of centroid δ_r. The travel distances δ_r evaluated from horizontal displacements of a center of gravity by simplify rigid block

model in **Fig. 8**. The Potential energy and energy ratio at TDL-N slide are calculated 932 kJ/m^2 and 11.7, respectively. An energy contributing for slope failure at TDL-N slide have resulted in using potential energy about 12 times larger than earthquake energy. These results were roughly approximated, indicating that the travel distance δ_r increase with an energy ratio.

Figure 14 shows the failed soil volumes V m^3 are plotted versus the friction coefficients back-calculated. On the same chart, it shows the friction coefficients and the failed soil volumes in large slope failures by Hsu, J. 1975. It has followed that the failed soil mass decreases with increasing the friction coefficient μ.

In **Figs. 12-14**, what is to be noted is that the failed mode Type-A has the slight difference between 2016 Kumamoto EQ.'s result and 2004 Niigata-ken Chuetu EQ.'s results. It can be presumed that the travelled soil mass of TLD-N site was stopped nearly 0^o after earthquake in **Fig. 8**, and the earthquake energy for slope failure during Kumotomo EQ. is larger than Chuetu EQ in that estimating a simple theory of spherical energy radiation for M=6.9 during 2004 Chuethu EQ.. In this respect, one interpretation of a failure mechanism at TLD-N site is that after the shear strength of soil along slip plane reduced drastically by seismically induced effects such as high water pressure acting on the slip plane, the failed soil mass travelled not inertial force but potential energy.

In order to upgrade the energy method to a reliable design tool, more research on model tests and case history studies for actual failures in complex in situ conditions are needed based on the back-calculation of friction coefficients in case histories.

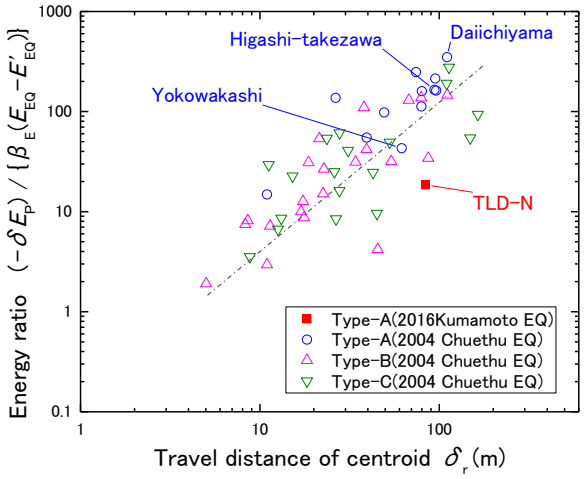

Fig. 13. Ration of Potential energy to Earthquake energy versus Travel distance of centroid

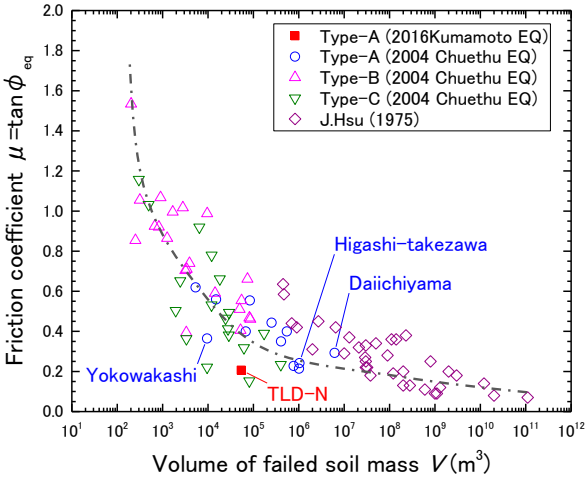

Fig. 14. Back-calculated friction coefficients versus volumes of failed soil mass

4. Conclusions

The energy approach to back-calculate the equivalent friction coefficients for slope failure during the 2016 Kumamoto earthquakes has yielded the following major findings:

1) The input energy E_{IP}/A during the 2016 Kumamoto earthquakes, puts its focus on calculated energy by strong motion sites around the Aso caldera, can be approximated by a simple theory of spherical energy radiation for M =7.1.
2) It was applied this energy evaluation method to the slope failure on northern side slope (TLD-N site) at the Takanoobane lava dome. Consequently, the back-calculated friction angle is much lower than the initial slope inclination.
3) The contributed energy for slope failure at TLD-N site(Type-A), displaced soil mass travelled gentle slope along the clearly slip plane, estimates the potential energy much larger than the earthquake energy.
4) From results of lower friction and larger potential energy for slope failure, it can be presumed that the shear strength of soil along slip plane reduced drastically by seismically induced effects such as high water pressure acting on the slip plane at TLD-N site.

Acknowledgements

Part of this study was supported by International Urgent Collaborative Projects regarding the 2016 Kumamoto Earthquake within the J-RAPID Program, "Mechanism of Fluidized Landslides due to 2016 Kumamoto Earthquake and Risk Evaluation of Unstable Soils- A Factual Investigation by Japan-USA Joint Research (Research leader:

Professor Hemanta Hazarika (Kyusyu University))" of Japan Science & Technology Agency. KIK-net data, DEM data and Air-photographs were obtained from the website of NIED (National Research Institute for Earth Science and Disaster Resilience) and GSI (Geospatial Information Authority of Japan). I am grateful to Dr. T.Danjo and Dr. T.Kimura (NIED) for helpful discussions.

References

Gutenberg, B. and Richter, C.F., 1956. Earthquake magnitude, intensity, energy and acceleration (Second paper), Bulletin of Seismological Society of America, **46**: 105–145.

Hsu, J., 1975. Catastrophic debris streams generated by rock falls 1975. Geological Society of America Bulletin, Doc.no. 50117, **86**: 129–140.

Kokusho, T. and Kabasawa, K., 2003. Energy approach to flow failure and its application to flow due to water film in liquefied deposits, Proc. of International Conference on Fast Slope Movement, Naples: 297-302.

Kokusho, T. and Ishizawa, T., 2007. Energy approach to earthquake-induced slope failures and its implications, Journal of Geotechnical and Geo-environmental Engineering, ASCE, **133** (7): 828–840.

Kokusho, T. and Suzuki, T., 2011. Energy flow in shallow depth based on vertical array records during recent strong earthquakes, Soil Dynamics & Earthquake Engineering, Elsevier: 1540-1550.

Kokusho, T., Koyanagi, T. and Yamada, T., 2014. Energy approach to seismically induced slope failure and its application to case histories -Supplement-, Engineering Geology, **181**: 290-296.

Symbols and abbreviations

D_{av}	Average thickness of sliding mass
du/dt	Particle velocity of the design motions in terms of time t
E_{DP}	Dissipated energy in soil due to the slope
E_{EQ}	Earthquake energy contributing to slope failure
E'_{EQ}	Earthquake energy for soil damping, liquefaction
E_{IP}	Input earthquake energy at the base of slopes
E_K	Kinetic energy in a sliding soil mass
E_{RD}	Radiation damping energy
M	Earthquake magnitude using Richter scale
Mg	Weight
M_J	JMA (Japan Meteorological Agency) magnitude
M_W	Moment magnitude
R	Hypocentral distance
R_0	Focal depth of the main shock
α	Impedance ratio
β	Slope inclination
β_0	Initial slope inclination
β_E	Energy ratio contributing to driving soil mass for downslope direction
$-\delta E_P$	Gravitational potential energy change
δ_r	Residual slope displacement
θ_0	Initial slope angle
μ	Equivalent friction coefficient
ρ	Soil density
$\rho \cdot V_S$	Impedance of the base layer
ϕ_{eq}	Equivalent friction angle